Color Snakes

Guillermo Sapiro
Hewlett-Packard Labs
1501 Page Mill Road
Palo Alto, CA 94304
guille@hpl.hp.com

August 31, 1995, submitted

Abstract

A framework for object segmentation in vector-valued images is presented in this paper. The scheme proposed is based on geometric active contours moving towards the objects to be detected in the color or vector-valued image. Objects boundaries are then obtained as geodesics or minimal weighted distance curves in a Riemannian space. The metric in this space is given by a definition of edges in vector-valued images. The curve flow corresponding to the proposed active contours holds formal existence, uniqueness, stability, and correctness results. Based on an efficient numerical algorithm for curve evolution, we present a number of examples of object detection in real color and texture images. These examples show the algorithm capability to automatically handle changes in the deforming curve topology. We conclude the paper presenting an extension of the color active contours which leads to a possible image flow for vector-valued image segmentation. The algorithm is based on moving each one of the image level-sets according to the proposed color active contours. This extension also shows the relation of the color geodesic active contours with a number of partial-differential-equations based image processing algorithms as anisotropic diffusion and shock filters.

Key words: Object segmentation, color images, textures, vector-valued images, vector edges, active contours, variational problems, differential geometry, Riemannian geometry, geodesics, topology free boundary detection, anisotropic diffusion.

1 Introduction

One of the basic problems in image analysis is object segmentation. Object detection and image segmentation has been studied since the early days of computer vision and image processing, and different approaches have been proposed; see for example [39, 61, 62, 108] and references therein. Object segmentation can be associated with the problem of boundary detection and integration, when boundary is roughly defined as a curve or surface separating "homogeneous" regions. Of course, a mathematical (and many times also perceptual) definition of homogeneity is the fundamental component of any segmentation algorithm.

"Snakes," or active contours, were proposed by Kass *et al.* [41] to approach this problem, and received a great deal of attention from the image analysis community since then. The work was later extended to 3D surfaces. The classical snakes approach, revisited in the following Section, is based on deforming an initial contour or surface towards the boundary of the object to be detected. The deformation is obtained by minimizing a global energy designed such that its (local) minima is obtained at the boundary of the object. These active surfaces are examples of the general technique of matching deformable models to image data by means of energy minimization [9, 97]. The energy is basically composed by a term which controls the smoothness of the deforming curve and another one that attracts it to the boundary. This model is not capable of changing its topology when direct implementations are performed. The topology of the final curve will be in general that of the initial one, unless special procedures are implemented for detecting possible splitting and merging points [59, 94]. See for example [8, 58, 107] and references therein for comments on advantages and disadvantages of energy approaches for deforming contours, as well as an extended literature on recent related works.

Geometric models of deformable contours and surfaces were simultaneously proposed by Caselles *et al.* [11] and by Malladi *et al.* [57, 58], and are also revisited in the following section. These models are based on the theory of surface evolution and geometric flows, which has gained a large amount of attention from the image analysis community in the past years [2, 3, 29, 30, 31, 44, 45, 46, 48, 64, 72, 77, 81, 83, 84, 85, 86, 95, 101]. In these models, the curve or surface is propagating (deforming) by an implicit velocity that also contains two terms, one related to the regularity of the deforming shape and the other attracting it to the boundary. The model is given by a geometric flow (PDE), based on mean curvature motion, and not by an energy function. This model allows automatic changes in topology when implemented using the level-sets numerical algorithm introduced by Osher and Sethian [69, 88, 89]. Thereby, several objects can be detected simultaneously, without previous knowledge of their exact number in the scene, and without special tracking procedures.

In [13], we showed the relation between these two approaches for two dimensional object detection (two dimensional curve evolution), proposing what we called "geodesic active contours." The work was extended to 3D based on the theory of minimal surfaces [71] in [14] (see also [42, 91]). We first proved that for a particular case, the classical energy snakes approach is equivalent to finding a geodesic curve in a Riemannian space with a metric derived from the grey-level image. This means that the boundary we are looking for is the path of minimal distance, measured in the Riemannian metric, that connects given image points. We then showed that assuming a level-set representation of the deforming contour, we can find this geodesic curve via a geometric flow which is very similar to the one obtained in the curve evolution approaches mentioned above. (The same flows were recently independently obtained in [42, 91]. See also [22, 101].) This flow, however, includes a new term that improves those models. (Although this term appears in similar forms in classical snakes, it was missing in curve evolution models. This term is naturally incorporated by the geodesic formulation.) The new term allows to track in an accurate way boundaries with high variation in their gradient, a task that was impossible with previous curve evolution models. We also showed that the solution of the flow exists in the viscosity framework, and is unique and stable. Therefore, the active contours approach presented in [13] has the following main properties: 1- Connects energy and curve evolution approaches of active contours. 2- Presents the snake problem as a geodesic computation one. 3- Improves existing models as a result of the geodesic formulation. 4- Allows simultaneous detection of interior and exterior boundaries in several objects without special contour tracking procedures. 5- Holds formal existence, uniqueness, and stability results. 6- Stops automatically.

In this paper we first extend the results in [13] to object detection in vector-valued images, presenting what we denote as "color snakes" ("color active contours"). [1] Vector-valued images are not just obtained in image modalities were the data is recorded in a vector fashion, as in color (RGB, luminance-chrominance), medical (MRI, X-ray, ultrasound) and LANDSAT applications. The vector-valued data can be obtained also from scale and orientation decompositions for texture analysis as in [6, 52, 107], or as a way to to improve color metrics [100]. The framework proposed in this paper applies to all these cases.

In general, two different approaches can be adopted to work on vector-valued images. The first approach is to process each plane separetly, with the geodesic active contours in [13] for example, and then to somehow integrate the results of this operation to obtain one unique segmentation for the whole image. The second approach is to integrate the vector information from the very beginning, and deform a unique curve based on this information, directly obtaining a unique object segmentation. The first approach suffers from three main problems: 1- Boundaries (objects) may be defined by the combination of the different planes and not by a plane in particular, or they may be missing in some planes. Examples of this are color images, where iso-luminance or iso-color areas show boundaries only in particular planes. 2- While different planes are in general highly correlated, as for example in color and medical images, this correlation is not used in the segmentation process. This correlation can help for example to avoid local minima due to noise. 3- The step of curve integration, being critical, is not trivial. For example, it is not clear how to integrate when boundaries appear only in a subset of the planes.

In this work, we adopt the second approach, that is, we integrate the original image information to find a unique segmentation directly. The main idea is to define a new Riemannian (metric) space based on information obtained from all the components in the image. More explicitly, edges are computed based on classical results on Riemannian geometry [50], following the developments in [24, 25, 82]. When the image components are correlated, as in color images, this approach is less sensitive to noise than the combination of scalar gradients obtained from each component [51]. These vector edges are used to define a new metric space on which the geodesic curve is to be computed. The object boundaries are then given by a minimal "color weighted" path. The resulting approach holds the properties mentioned above for the geodesic active contours developed in [13].

We then extend the color active contours to obtain an approach for combined color anisotropic diffusion and shock filtering of vector-valued images, leading to a possible image flow for segmentation/simplification. This is based on moving all the level-sets of the image according to the color geodesic snakes. The resulting flow, denoted as *color self-snakes*, is closely related to a number of previously reported image processing algorithms based on PDE's, as anisotropic diffusion [3, 15, 74] and shock-filters [70], as well as the Mumford-Shah variational approach for image segmentation [62, 90]. (Relations between a number of those

[1] In this paper we use the word "color" to refer to general multi-valued images.

PDE-based approaches were previously also reported in [2, 4, 106]. Here (and in [12]) we add the (color) geodesic snakes to the connection.) These relations, as well as examples for color images, are described in this paper. More examples and details on self-snakes for grey-level (single-valued) data can be found in [12].

We should mention that a number of results on color or vector-valued segmentation were reported previously in the literature; see for example [52, 73, 107]. Here we address the geodesic active contours approach with vector-image metrics. Other algorithms can be extended as well to work on vector-valued images following the framework described in this paper.

This paper is organized as follows. In Section 2 we briefly review both classical energy based and curve evolution based deformable models. In Section 3 we describe the main results on 2D geodesic active contours as presented in [13]. In Section 4 we deal with the computation of edges in vector-valued images, following [82]. The vector-valued active contours are then presented in Section 5. Here we present theoretical results regarding the proposed model as well. Experimental results on the color snakes are given in Section 5.2. The color self-snakes are described in Section 6. Discussion and concluding remarks are given in Section 7.

2 Basic approaches on active contours

2.1 Energy based snakes

Let $\mathcal{C}(p) : [0, 1] \to I\!R^2$ be a parametrized planar curve, and $I : [0, a] \times [0, b] \to I\!R^+$ a given image where we want to detect the objects boundaries. The classical snakes approach [41] associates to the curve $\mathcal{C}$ an energy given by

$$E(\mathcal{C}) = \alpha \int_0^1 |\mathcal{C}'(\tau)|^2 d\tau + \beta \int_0^1 |\mathcal{C}''(\tau)|^2 d\tau - \lambda \int_0^1 |\nabla I(\mathcal{C}(\tau))| d\tau, \qquad (1)$$

where α, β, and λ are real positive constants (α and β impose the elasticity and rigidity of the curve). The first two terms basically control the smoothness of the contours to be detected (internal energy), while the third term is responsible for attracting the contour towards the object in the image (external energy). Solving the problem of snakes amounts to finding, for a given set of constants α, β, and λ, the curve $\mathcal{C}$ that minimizes E. Note that when considering more than one object in the image, and for example the initial prediction of $\mathcal{C}$ surrounds all of them, it is not possible to detect all the objects in a straightforward form. In other words, a direct implementation of the classical (energy) approach of snakes can not deal with changes in topology, unless special topology handling procedures are added [59, 94]. The topology of the initial curve will be the same as the one of the (possible wrong) final solution. The models in [11, 13, 42, 57, 58, 95, 101] automatically overcome this problem.

It is clear that the classical snakes method can be generalized to 3D data images, where the boundaries of the objects are surfaces. This extension is known as the deformable surfaces model, and was introduced by Terzopoulos *et al.* [97] for a 3D representation of objects and extended and used by many others (see for example [19, 20, 21, 60, 96]).

This is the basic formulations of 2D energy based snakes. Other related formulations have been proposed in the literature. Reviewing all of them is out of the scope of this paper.

2.2 Deformable models based on curvature motion

Recently, novel geometric models of deformable curves were simultaneously proposed by Caselles *et al.* [11] and by Malladi *et al.* [57, 58]. Assume in the 2D case that the deforming curve $\mathcal{C}$ is given as a level-set of a function $u : I\!R^2 \to I\!R$. Then, we can represent the deformation of $\mathcal{C}$ via the deformation of u. In this case, the proposed 2D deformation is given by

$$\frac{\partial u}{\partial t} = g_{grey}(I)|\nabla u|\mathrm{div}\left(\frac{\nabla u}{|\nabla u|}\right) + \nu g_{grey}(I)|\nabla u| \qquad (t,x) \in [0,\infty[\times I\!R^2 \tag{2}$$

$$u(0,x) = u_0(x) \qquad x \in I\!R^2 \tag{3}$$

where ν is a positive real constant,

$$g_{grey}(I) = \frac{1}{1 + |\nabla \hat{I}|^p}, \tag{4}$$

$\hat{I}$ being a regularized version of the original image I where we are looking for the contour of an object O, and $p = 1$ or 2. Typically, the initial condition $u(0,x) = u_0(x)$, in the case of outer snakes (curves evolving towards the boundary of O from the exterior of O), is taken as a regularized version of $1 - \chi_C$ where χ_C is the characteristic function of a set $\mathcal{C}$ containing O. Using the fact that

$$\mathrm{div}\left(\frac{\nabla u}{|\nabla u|}\right) = \kappa,$$

where κ is the Euclidean curvature [26, 37] of the level-sets $\mathcal{C}$ of u, Equation (2) can then be written in the form

$$u_t = g_{grey}(I)(\nu + \kappa)|\nabla u|.$$

Equation (2) can be interpreted as follows: Suppose that we are interested in following a certain level-set of u, which to fix ideas we suppose to be the zero level-set. Suppose also that this level-set is a smooth curve. Then the flow

$$u_t = (\nu + \kappa)|\nabla u|,$$

means that the level-set $\mathcal{C}$ of u we are considering is evolving according to

$$\mathcal{C}_t = (\nu + \kappa)\vec{\mathcal{N}}, \tag{5}$$

where $\vec{\mathcal{N}}$ is the inward normal to the curve. [2] This equation was first studied in [69, 88, 89], where extensive numerical research on it was performed, introducing the level-sets curve evolution approach. It was introduced in computer vision in [44, 45], where deep research for shape analysis was performed, presenting a novel geometric scale-space for planar shape analysis and decomposition among other things.

[2] Based on the fact that $\vec{\mathcal{N}} \parallel \nabla u$, it is straightforward to prove that when the level-sets $\mathcal{C}$ of u evolve according to $\mathcal{C}_t = \beta\vec{\mathcal{N}}$, the function u should deform via $u_t = \beta|\nabla u|$ when the level-sets approach is well posed.

The motion

$$\mathcal{C}_t = \kappa\vec{\mathcal{N}},$$

denoted as *Euclidean heat flow* is very well know for its geometric smoothing properties [5, 34, 36]. (This flow was extended in [83, 84, 85] for the affine group and in [67, 85] for others. See also [29, 30] for the projective group.) This flow is also called the *Euclidean shortening flow*, since it moves the curve in the gradient direction of the length functional given by

$$L := \oint_{\mathcal{C}} ds, \tag{6}$$

where $ds = |\mathcal{C}_p|dp$ is the Euclidean arc-length element. Therefore, this flow decreases the length of the curve as fast as possible. This property is important for the geometric interpretation of the geodesic models in this paper.

The constant velocity $\nu\vec{\mathcal{N}}$ in (5), which is related with classical mathematical morphology [44, 45, 81], acts as the balloon force in [20]. Actually this velocity pushes the curve inwards and it is crucial in the model in order to allow convex initial curves to become non-convex, and thereby detect non-convex objects. This is necessary because a convex curve remains convex when evolving according to the Euclidean heat flow [34]. Of course, the ν parameter must be specified a priori in order to make the object detection algorithm automatic. This is not a trivial issue, as pointed out in [11], where possible ways of estimating this parameter are considered. A probabilistic approach for selecting ν that can be adapted to this framework was recently proposed in [107]. Recapping, the "force" $(\nu + \kappa)$ acts as the internal force in the classical energy based snakes model. The external force is given by $g_{grey}(I)$, which is supposed to prevent the propagating curve from penetrating into the objects in the image. In [11, 57, 58], the authors choose $g_{grey}(I)$ given by (4). $\hat{I}$ was smoothed using Gaussian filtering, but more effective geometric smoothers can be used as well [62]. Note that other decreasing functions of the gradient may be selected as well. For an ideal edge, $\nabla\hat{I} = \delta$, $g_{grey} = 0$, and the curve stops at the edge ($u_t = 0$). The boundary is then given by the set $u = 0$.

This curve evolution model given by (2) automatically handles different topologies. That is, there is no need to know a priori the topology of the solution. This allows to detect any number of objects in the image, without knowing their exact number. This is achieved with the help of the efficient level-sets numerical algorithm for curve evolution, developed by Osher and Sethian [69, 88, 89], and used by others for different image analysis problems [18, 44, 45, 48, 81, 84, 86], and analyzed for example in [17, 28]. In this case, the topology changes are automatically handled, without the necessity for specific monitoring the topology of the deforming curve.

3 Geodesic active contours

We now review the main results of [13]. Let us consider a particular case of (1), where $\beta = 0$. Two main reasons motivate this selection: First, it allows to derive the relation between energy based active contours and geometric curve evolution ones. Second, although having $\beta \neq 0$ adds flexibility and other properties, the regularization effect on the geodesic active contours comes from curvature based curve flows, obtained only from the other terms in (1). This allows to achieve smooth curves in the proposed approach without having the high order derivatives given by $\beta \neq 0$. The use of the curvature driven curve motions for smoothing was proved to be very efficient in previous works [2, 11, 44, 45, 58, 77, 84], and is also supported by our experiments in [13] and Section 5.2. Therefore, curve smoothing will be obtained also with $\beta = 0$, keeping only the first regularization term. Assuming this, and replacing the edge detector $|\nabla I|$ by a general function $g_{grey}(|\nabla I|)^2$ of the gradient such that $g_{grey}(r) \rightarrow 0$ as $r \rightarrow \infty$, we obtain,

$$E(\mathcal{C}) = \alpha \int_0^1 |\mathcal{C}'(\tau)|^2 d\tau + \lambda \int_0^1 g_{grey}(|\nabla I(\mathcal{C}(\tau))|)^2 d\tau = E_{int}(\mathcal{C}) + E_{ext}(\mathcal{C}). \tag{7}$$

(In order to simplify the notation, we sometimes write $g_{grey}(I)$ or $g_{grey}(\mathcal{X})$ ($\mathcal{X} \in I\!R^2$) instead of $g_{grey}(|\nabla I|)$.) The goal now is to minimize E in (7) for $\mathcal{C}$ in a certain allowed space of curves. Of course, in (7), only the ratio λ/α counts.

As argued in [13], the functional (7) is not intrinsic, it depends on the parametrization of the curve. This could be considered as an undesirable property since parametrizations are not related to the geometry of the curve (or object boundary), but only to the velocity they are traveled. Motivated by the discussion on ideal edges, in [13] we proposed to fix this degree of freedom by fixing the energy level $E_0 = 0$ at the local minima (other values are analyzed in [13] as well). Then with the help of Maupertuis' and Fermat Principles [27], we proved that the solution of (7) is given by a geodesic curve in a Riemannian space. The metric in this Riemannian space is defined by $g_{ij}\, dx_i dx_j$ with $g_{ij} = g_{grey}(I)^2 \delta_{ij}$. This means that the object is detected when a curve of minimal length is found. In other words, we proved that under these conditions, minimizing (7) is equivalent to solving

$$\mathrm{Min}_{\mathcal{C}} \int_0^1 g_{grey}(|\nabla I(\mathcal{C}(\tau))|)|\mathcal{C}'(\tau)| d\tau. \tag{8}$$

We have transformed the problem into a problem of geodesic computation in a Riemannian space, according to a new metric (length measure) given by

$$L_R := \int_0^1 g_{grey}(|\nabla I(\mathcal{C}(\tau))|)|\mathcal{C}'(\tau)| d\tau. \tag{9}$$

Since $|\mathcal{C}'(\tau)|d\tau = ds$ (Euclidean arc-length), we may write

$$L_R := \int_0^L g_{grey}(|\nabla I(\mathcal{C}(\tau))|) ds.$$

where L denotes the Euclidean length of $\mathcal{C}(\tau)$. Comparing this with the classical Euclidean length as given in previous section by (6), we find that the new length is obtained by weighting ds with $g_{grey}(|\nabla I(\mathcal{C})|)$, which contains information regarding the boundary of the object. Therefore, when trying to detect an object, we are not just interested in finding the path of minimal classical length ($\oint ds$) but the one which minimizes a new definition of length which takes into account image characteristics. Note that (8) is general, no assumptions on g_{grey} were done, besides being a decreasing function. For example, g_{grey} can be derived from edge-type maps as those in [49]. Therefore, the theory of detection based on geodesic computations given above, and fully described in [13], is general. This is fundamental for the "color active contours" developed in this paper; Section 5.

In order to find this geodesic curve, we use the steepest descent method which will give us a local minima of (9). Then, the flow minimizing L_R is given by [13]

$$\mathcal{C}_t = (g_{grey}\kappa - \nabla g_{grey} \cdot \vec{\mathcal{N}})\vec{\mathcal{N}} \tag{10}$$

We now introduce the level-set formulation [69, 88, 89] in the model. Let us assume that a curve $\mathcal{C}$ is parametrized as a level-set of a function $u : [0,a] \times [0,b] \to I\!R$. That is, $\mathcal{C}$ is such that it coincides with the set of points in u such that $u =$ constant. In particular given an initial curve $\mathcal{C}_0$ we parametrize it as a zero level-set of a function u_0. Then, the level-set formulation of the steepest descent method says that solving the above geodesic problem starting from $\mathcal{C}_0$ amounts to searching for the steady state ($\frac{\partial u}{\partial t} = 0$) of the following evolution equation:

$$\begin{aligned} \frac{\partial u}{\partial t} &= |\nabla u| \mathrm{div}\left(g_{grey}(I) \frac{\nabla u}{|\nabla u|} \right) \\ &= g_{grey}(I)|\nabla u| \mathrm{div}\left(\frac{\nabla u}{|\nabla u|} \right) + \nabla g_{grey}(I) \cdot \nabla u, \end{aligned} \tag{11}$$

with initial datum $u(0,x) = u_0(x)$. This equation is then obtained by computing the gradient descent of L_R and embedding the flow as the level-set of u. We have obtained the main part of the geodesic active contours.

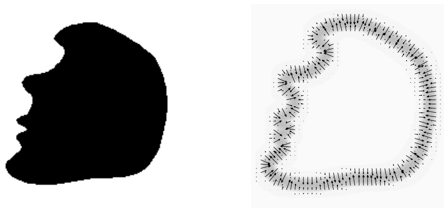

Figure 1: Geometric interpretation of the new term in the geodesic deformable model. The gradient vectors are all directed towards the middle of the boundary. Those vectors direct the propagating curve into the valley of the g_{grey} function.

Comparing Equation (11) to (2), we first observe that the term $\nabla g_{grey} \cdot \nabla u$ is missing in the old model. This is due the fact that in (2), a classical length in Euclidean space is used (given by (6)). In the new model, the length takes into account the image structure, and is given by (9), defining a new Riemannian space. This new term directs the curve towards the boundary of the objects, the valley of g_{grey}. This is demonstrated in Figure 1. This new force increases the attraction of the deforming contour towards the boundary, being of special help when the boundary has high variations of its gradient values. Note that in the old model, the curve stops when $g_{grey} = 0$. This happens only along an ideal edge. Also, if there are different gradient values along the edge, as it often happens in real images, then g_{grey} gets different values at different locations along the object boundaries. It is necessary to consider all those values as high enough to guarantee the stopping of the propagating curve. This makes the geometric model (2) inappropriate for the detection of boundaries with (un-known) high variations of the boundary gradients. In our new model, we have both a stopping term and an attraction one. Thereby, it is also possible to detect boundaries with high differences in their gradient values. The second advantage of this new term is that we partially remove the necessity of the constant velocity given by ν. This constant velocity, that mainly allows the detection of non-convex objects, introduces an extra parameter to the model, that in most cases is an undesirable property. In our case, the new term allows the detection of non-convex objects as well. This term also helps when starting from curves inside the object. In case we wish to add this constant velocity, in order for example to increase the speed of convergence, we can just consider the term $\nu g_{grey}(I)|\nabla u|$ as an extra speed (which minimizes the enclosed area [20, 107]), in the geodesic problem (8) obtaining

$$\frac{\partial u}{\partial t} = |\nabla u| \mathrm{div}\left(g_{grey}(I) \frac{\nabla u}{|\nabla u|} \right) + \nu g_{grey}(I)|\nabla u|. \tag{12}$$

This equation is of course equivalent to

$$\frac{\partial u}{\partial t} = g_{grey}(\nu + \kappa)|\nabla u| + \nabla u \cdot \nabla g_{grey}. \tag{13}$$

Equation (12), which is the solution of the geodesic problem (8) with an extra area-based speed, constitutes the *geodesic active contours*. As shown in the examples in [13], it is possible to choose $\nu = 0$ (no constant velocity), and the model still converges in general to the correct solution (in a slower motion). The advantage is that we have obtained a model with less parameters.

This equation, as well as its 3D extension [14], was independently proposed by Kichenassamy *et al.* [42] based on a slightly different initial approach. The authors in [42] derived (8) motivated by gradient flows and the work in [11, 57], without showing its connection with classical snakes as done in [13]. Of course, once (8) is obtained, (12) is derived, obtaining in [42] the same curve flow. Shah [91] also recently presented an active contours formulation using a weighted length formulation as in (8) as starting point. In his case, g_{grey} is obtained from an elaborated segmentation procedure obtained from the Mumford-Shah approach [62]. Extensions of the model in [11, 57] are studied also in [95] motivated in part by the work in [44, 45]. In [101] (see also [102]), related 3D models are studied as well. Minimization of a normalized version of L_R was proposed in [33] from a different perspective, leading to a different geometric method.

4 Vector-valued edges

We present now the definition of edges in vector-valued images, based on classical Riemannian geometry results [50]. The basic goal is to extend edge detectors for 2D and 3D single-valued data [10, 109] to vector-valued images.

The Riemannian geometry framework for edge detection in multi-valued images described below was first suggested in [25]. Other approaches to vector-valued edge detectors consist in combining the response of single-valued edge detectors applied separately to each of the image components (see for example [63]). The way the responses at each plane are to be combined is in general heuristic and has no theoretical basis. The Riemannian space approach has a solid theoretical background and constitutes a consistent extension of single-valued gradient computations. Di Zenzo applied these ideas to edge detection in color RGB space. Although the work by Di Zenzo is performed assuming an Euclidean metric, which is not perceptually correct in the RGB space, the basis given in [25] can be extended to other spaces and/or other metrics as we explain below.

In [24], Cumani extended the analysis of the first fundamental form (see below) applied to edge detection in multi-valued images. He analyzed the directional derivative of the maximal change value (see below), in the direction of this change, defining an edge as a zero crossing of this function. This work attempts to extend the ideas in [98] developed for single-valued images. Cumani analyzed edges of multi-valued functions by means of transversal zero crossings of the derivatives of this maximal change value alone. As we argue below, for vector-valued edges, the relation between the maximal and minimal changes should be analyzed. Analysis was carried out in [24] concerning the characteristics and topology of the zero crossing sets.

Noise analysis of the vector-valued edge detector was performed in [51]. The authors showed that for correlated data, this edge detector as presented below is more stable to noise than the simple combination of the gradient components.

We derive now these ideas, following [82]. Let $\Phi(u_1, u_2) : I\!R^2 \to I\!R^m$ be a multi-valued image with components $\Phi_i(u_1, u_2) : I\!R^2 \to I\!R$, $i = 1, 2, ..., m$. For color images we have $m = 3$ components. The value of the image at a given point (u_1^0, u_2^0) is a vector in R^m, and the difference of image values at two points $P = (u_1^0, u_2^0)$ and $Q = (u_1^1, u_2^1)$ is given by

$$\Delta\Phi = \Phi(P) - \Phi(Q).$$

When the (Euclidean) distance $d(P, Q)$ between P and Q tends to zero, the difference becomes the arc element

$$d\Phi = \sum_{i=1}^{2} \frac{\partial \Phi}{\partial u_i} du_i, \tag{14}$$

and its squared norm is given by

$$d\Phi^2 = \sum_{i=1}^{2} \sum_{j=1}^{2} \frac{\partial \Phi}{\partial u_i} \frac{\partial \Phi}{\partial u_j} du_i du_j. \tag{15}$$

This quadratic form is called the *first fundamental form* [50]. Although we present now only the Euclidean case, the theory we develop holds for any non-singular Riemannian metric in the space. For different metrics, either a space transform can be applied to an Euclidean space if possible, or the metric induced by the given space can be used directly (if it is non-singular). This is particularly useful for color images, as all the line element theories of color vision [105] can easily be incorporated in our scheme.

Using the standard notation of Riemannian geometry [50], we have that

$$g_{ij} := \frac{\partial \Phi}{\partial u_i} \cdot \frac{\partial \Phi}{\partial u_j},$$

and

$$d\Phi^2 = \sum_{i=1}^{2} \sum_{j=1}^{2} g_{ij} du_i du_j = \begin{bmatrix} du_1 \\ du_2 \end{bmatrix}^T \begin{bmatrix} g_{11} \, g_{12} \\ g_{21} \, g_{22} \end{bmatrix} \begin{bmatrix} du_1 \\ du_2 \end{bmatrix}. \tag{16}$$

For a unit vector $\hat{v} = (v_1, v_2) = (\cos\theta, \sin\theta)$, $d\Phi^2(\hat{v})$ indicates the rate of change of the image in the $\hat{v}$ direction. It is well known that the extrema of the quadratic form (16) are obtained in the directions of the eigenvectors of the metric tensor $[g_{ij}]$, and the values attained there are the corresponding eigenvalues. Simple algebra shows that the eigenvalues are

$$\lambda_\pm = \frac{g_{11} + g_{22} \pm \sqrt{(g_{11} - g_{22})^2 + 4g_{12}^2}}{2}, \tag{17}$$

and the eigenvectors are $(\cos\theta_\pm, \sin\theta_\pm)$ where the angles $\theta_\pm$ are given (modulo π) by

$$\theta_+ = \frac{1}{2}\mathrm{arctan}\frac{2g_{12}}{g_{11} - g_{22}}, \tag{18}$$

$$\theta_- = \theta_+ + \pi/2. \tag{19}$$

The eigenvectors provide the direction of maximal and minimal changes at a given point in the image, and the eigenvalues are the corresponding rates of change. We call θ_+ the *direction of maximal change* and λ_+ the *maximal rate of change*. Similarly, θ_- and λ_- are the *direction of minimal change* and the *minimal rate of change* respectively. Note that for $m = 1$, that is, for grey-level images, $\lambda_+ \equiv \| \nabla\Phi \|^2$, $\lambda_- \equiv 0$, and $(\cos\theta_+, \sin\theta_+) \parallel \nabla\Phi$.

In contrast with grey-level images ($m = 1$), the minimal rate of change λ_- may be different than zero. In the single-valued case, the gradient is perpendicular to the level-sets, and $\lambda_- \equiv 0$. The "strength" of an edge in the multi-valued case is not given simply by the rate of maximal change, λ_+, but by how λ_+ compares to λ_-. Therefore, a first approximation of edges for vector-valued images, analogue to selecting a function of $\| \nabla\Phi \|$ in the $m = 1$ case, should be a function $f = f(\lambda_+, \lambda_-)$. Selecting $f = f(\lambda_+ - \lambda_-)$ is one choice, since for $m = 1$ it reduces to the gradient-based edge detector.

Before concluding this section we should point out that based on the theory above, improved edge detectors for vector-valued images can be obtained following for example the developments on energy-based edge detectors [32, 75]. In order to present the color snakes, the theory developed above is sufficient.

4.1 Anisotropic diffusion of multi-valued images

In many applications, noise is removed before edge maps are computed. This is done while computing g_{grey} in (4) for example. It is desirable that the smoothing operation does not affect salient edges. For this, a number of schemes for anisotropic diffusion were recently developed [3, 74, 79]. We briefly review now the scheme for anisotropic diffusion of vector-valued images proposed in [82]. This flow will be used to compute the vector-valued metric in the color snakes developed below. The main goal of the work in [82] was to extend the results in [3] to vector-valued images. The work in [74] was extended for these type of data in [103]. Related work is reported in [16].

Given the directions $\theta_{\pm}$, we proceed to derive the corresponding anisotropic diffusion. This is done in an analogous way to the single-valued case discussed in [3]. Diffusion occurs normal to the direction of maximal change θ_{+} (i.e., in the direction perpendicular to the color edge) which, in our case, is given by θ_{-}. Thus, we obtain

$$\frac{\partial \Phi}{\partial t} = \frac{\partial^2 \Phi}{\partial \theta_{-}^2}, \tag{20}$$

which is equivalent to

$$\begin{bmatrix} \frac{\partial \Phi_1}{\partial t} \\ \cdot \\ \cdot \\ \cdot \\ \frac{\partial \Phi_m}{\partial t} \end{bmatrix} = \begin{bmatrix} \frac{\partial^2 \Phi_1}{\partial \theta_{-}^2} \\ \cdot \\ \cdot \\ \cdot \\ \frac{\partial^2 \Phi_m}{\partial \theta_{-}^2} \end{bmatrix}.$$

In order to have control over the local diffusion coefficient we add a factor g_{color} similar to the one proposed in [3] for single-valued images. Based on the same arguments as in last Section, g_{color} should be an inverse function of the relation between λ_{+} and λ_{-}, obtaining

$$\frac{\partial \Phi}{\partial t} = g_{color}(\lambda_{+}, \lambda_{-}) \frac{\partial^2 \Phi}{\partial \theta_{-}^2}, \tag{21}$$

A suitable choice for g_{color} is any decreasing function of the difference $(\lambda_{+} - \lambda_{-})$. The values $\lambda_{\pm}$ can be computed based on a smoothed estimate of Φ.

Before concluding this Section, let us make some further remarks on the use of the results above in different related frameworks. Since a function of the type $f = f(\lambda_{\pm})$ (e.g., $f = f(\lambda_{+} - \lambda_{-})$) becomes the vector-images replacement of $\| \nabla \Phi \|$ for single-valued images ($m = 1$), as pointed out in [82], image processing algorithms for single-valued images based on $\| \nabla \Phi \|$ can be basically extended to vector-images replacing the gradient by $f(\lambda_{\pm})$. An example of this is the color snakes and self-snakes developed in following Sections. Other examples include the *total variation* algorithm developed by Rudin *at al.* [79] (see also [7, 35]) for image denoising and the Mumford-Shah segmentation approach [62] (see also for a very interesting extension to vector images applied to textures the work by Lee, Mumford, and

Yuille [52]). In the case of the total variation denoising, Rudin *et al.* propose to minimize (under certain constraints) the functional

$$\int_\Omega \| \nabla\Phi \| \, dxdy.$$

Of course, norms different from the L^1 can be used as well (see [7, 35]), but this norm proved to give good results. The extension of this to vector-valued images will be

$$\int_\Omega f(\lambda_\pm) dxdy,$$

being this the *vector-valued total variation.* The flavor of this variational approach to vector-valued image denoising is very similar to the anisotropic diffusion described above, giving also a system of coupled PDE's when the gradient-descent approach is used. Research in this direction includes not only showing the algorithmic potential of the techniques, but also proving analogues to the extended theoretical results reported for example in [53, 62], as well as its numerical investigation. [3]

4.2 Metrics of color images

From the results presented above, having a metric in the vector-valued image, we can obtain the direction and values of maximal and minimal changes, and from them, define edges. Since color images ($m = 3$) will provide the basic examples used to demonstrate the vector-valued snakes proposed in next Section, we conclude the current Section with a brief description of perceptual color metrics.

One approach (the empirical method) in the search for a perceptually uniform color space is to experimentally measure psychophysical human thresholds (or iso-performance surfaces) from a reference point in different directions in color space [105]. This defines the local Riemannian metric at the reference point. This kind of measurement has to be repeated at different positions in color space. The method has been pioneered by MacAdam [54]. An alternative approach has been to develop theoretical models of human detection of color differences based on our knowledge of the physiology and psychophysics of the visual system [40, 87, 93, 99]. The predictions of these *line element models* provide the metric of the color space. In general, all the line element models derived from simple theoretical assumptions fail to represent many of the important features present in empirical data. Our algorithm can easily incorporate any of the empirical or theoretical line element models mentioned above (empirical data, however, has to be interpolated to cover the entire space).

The approach followed in this paper is the one in [82], to adopt one of the CIE standards that attempts to achieve an approximate uniform color space (in which color threshold surfaces are roughly spherical) under the observing conditions usually found in practice. We use the CIE 1976 $L^*a^*b^*$-space [105] with its associated color difference formula (which is simply the Euclidean distance in the space). The white reference point (X_w, Y_w, Z_w) is taken as the one obtained when the R, G, and B guns are driven to half of their maximum amplitude. That is, for a 256 values per color image, $(X_w, Y_w, Z_w) = (128, 128, 128)$. More specifically,

[3] The vector-valued total variation and its numerical analysis is currently being investigated in collaboration with T. Chan from UCLA and B. Rogoff from Stanford University.

the transform from RGB space the $L^*a^*b^*$ space is given by first a linear transform from RGB to XYZ space.

$$\begin{bmatrix} X_w X \\ Y_w Y \\ Z_w Z \end{bmatrix} = \begin{bmatrix} 0.0289 & 0.0406 & 0.0256 \\ 0.0165 & 0.0782 & 0.0129 \\ 0.0015 & 0.0140 & 0.1326 \end{bmatrix} \begin{bmatrix} R \\ G \\ B \end{bmatrix}.$$

Then, defining

$$f(r) := \begin{cases} r^{1/3} & \text{if } r > 0.008856 \\ 7.787r + 16.0/116.0 & \text{else,} \end{cases}$$

we obtain that the perceptually uniform color space $L^*a^*b^*$ is given by

$$L^* = \begin{cases} 116.0 * f(Y) - 16.0 & \text{if } Y > 0.008856 \\ 903.3 * Y & \text{else,} \end{cases}$$

$$a = 500.0(f(X) - f(Y)),$$

$$b = 200.0(f(Y) - f(Z)).$$

Note that in contrast with common luminance-chrominance spaces used for example for image compression (YCbCr, YUV), the relation between RGB and $L^*a^*b^*$ is non-linear.

The $L^*a^*b^*$ space is a first approximation to a perceptually uniform color spaces. More accurate approximations can be obtained for example taking into account spatial frequencies [100]. In this case, a new vector-valued image is obtained with $m > 3$, and the same theory presented above can be applied.

5 Color snakes

We present now the formulation of the *color snakes* or *color active contours.*

Let $f_{color} = f(\lambda_+, \lambda_-)$ be the edge detector as defined in Section 4. The edge stopping function g_{color} is then defined such that $g_{color} \to 0$ when $f \to \max(\infty)$, as in the grey-scale case. For example, we can choose

$$f_{color} := (\lambda_+ - \lambda_-)^{1/p} \quad \text{or} \quad f_{color} := \sqrt{\lambda_+},$$

$p > 0$, and

$$g_{color} := \frac{1}{1+f},$$

or

$$g_{color} := \exp\{-f\}.$$

The function (metric) g_{color} defines the Riemannian space on which we compute the geodesic curve. Defining

$$L_{color} := \int_0^L g_{color}\, ds, \tag{22}$$

the object detection problem in vector-valued images is associated with minimizing L_{color}. This is in analogy to the minimization of L_R given by (9) for the single-valued case. We have therefore formulated the problem of object segmentation in vector-valued images as a problem on finding a geodesic curve in a Riemannian space defined by a metric induced from the whole vector image. Note that two closely related Riemannian spaces are involved in this approach. The first is the one induced from the *line elements*, that is, is obtained from the metric measuring differences in the vector image. From this one, $\lambda_\pm$ are obtained. The second one is defined by the metric g_{color}. Since g_{color} is a function of $\lambda_\pm$, which are of course functions of the metric that defines differences in the image, both Riemannian spaces are related. Actually, their metrics are functions one of the other.

In order to minimize L_{color}, that is the *color length*, we compute as before the gradient descent flow. As pointed out before, the equations developed in Section 3 for the geodesic active contours are independent of the specific selection of the function g. Therefore, the same equations hold here, replacing g_{grey} by g_{color}. We then obtain from (10) the following minimizing flow:

$$\mathcal{C}_t = (g_{color}\kappa - \nabla g_{color} \cdot \vec{\mathcal{N}})\vec{\mathcal{N}}. \tag{23}$$

As before, although not completely necessary, we can add a constant force minimizing the enclosed area in order for example to speed up the convergence, obtaining

$$\mathcal{C}_t = (g_{color}(\nu + \kappa) - \nabla g_{color} \cdot \vec{\mathcal{N}})\vec{\mathcal{N}}. \tag{24}$$

Embedding now the evolving curve $\mathcal{C}$ in the function $u : \mathbb{R}^2 \to \mathbb{R}$ we obtain the general flow for the *color snakes*,

$$\frac{\partial u}{\partial t} = g_{color}(\nu + \kappa)|\nabla u| + \nabla u \cdot \nabla g_{color}. \tag{25}$$

Recapping, Equation (25) is the level-sets flow corresponding to the gradient descent of L_{color}. Its solution (steady-state) is a geodesic curve in the Riemannian space define by the metric $g_{color}(\lambda_\pm)$ of the vector-valued image. This solution gives the boundary of objects in the scene. Note that $\lambda_\pm$ can be computed on a smooth image obtained from the vector-valued anisotropic diffusion described above.

5.1 Existence and uniqueness of the flow

We present now a number of theoretical results regarding the color geodesic flow (25). These results are proved in [13, 14] for the 2D geodesic flow of single-valued images and the 3D minimal surfaces one. Therefore, we present them here without proofs. Existence is also proved in [43]. See the mentioned references for details.

With the notion of viscosity solutions [23], we can present the following result regarding our color geodesic model:

Theorem 1 *Let* $\mathrm{W}^{1,\infty}$ *denote the space of bounded Lipschitz functions in* $\mathbf{R}^2$. *Assume that* $g_{color} \geq 0$ *is such that* $\sup_{\mathcal{X}\in\mathbf{R}^2} |Dg_{color}^{1/2}(\mathcal{X})| < \infty$ *and* $\sup_{\mathcal{X}\in\mathbf{R}^2} |D^2 g_{color}(\mathcal{X})| < \infty$. *Let* $u_0 \in \mathrm{BUC}(\mathbf{R}^2) \cap \mathrm{W}^{1,\infty}(\mathbf{R}^2)$. *Then*

1. *Equation (25) admits a unique viscosity solution*

$$u \in \mathrm{C}([0,\infty) \times \mathbf{R}^2) \cap L^\infty(0,T; W^{1,\infty}(\mathbf{R}^2)) \text{ for all } T < \infty.$$

   Moreover, u satisfies

$$\inf u_0 \leq u(t,\mathcal{X}) \leq \sup u_0.$$

2. *Let* $v \in \mathrm{C}([0,\infty) \times \mathbf{R}^2)$ *be the viscosity solution of (25) corresponding to the initial data* $v_0 \in \mathrm{C}(\mathbf{R}^2) \cap \mathrm{W}^{1,\infty}(\mathbf{R}^2)$. *Then*

$$\| u(t,\cdot) - v(t,\cdot) \|_\infty \leq \| u_0 - v_0 \|_\infty \text{ for all } t \geq 0.$$

   This shows that the unique solution is stable.

In the next Theorem, we recall results on the independence of the generalized evolution with respect to the embedding function u_0. Let Γ_0 be the initial active contour, oriented such that it contains the object. In this case the initial condition u_0 is selected to be the signed distance function, such that it is negative in the interior of Γ_0 and positive in the exterior. Then, we have

Theorem 2 (Theorem 7.1, [17]) *Let* $u_0 \in W^{1,\infty}(\mathbf{R}^2) \cap \mathrm{BUC}(\mathbf{R}^2)$. *Let* $u(t,x)$ *be the solution of the proposed geodesic evolution equation as in previous theorem. Let* $\Gamma(t) := \{\mathcal{X} : u(t,\mathcal{X}) = 0\}$ *and* $\mathcal{D}(t) := \{\mathcal{X} : u(t,\mathcal{X}) < 0\}$. *Then,* $(\Gamma(t), \mathcal{D}(t))$ *are uniquely determined by* $(\Gamma(0), \mathcal{D}(0))$.

Further properties of the level-sets flow can be proved based on the results in [28, 92]. See [13].

To conclude this section, let us mention that, in the case of a smooth ideal edge $\hat{\Gamma}$, one can prove that the generalized motion $\Gamma(t)$ converges to $\hat{\Gamma}$ as $t \to \infty$, making the proposed approach consistent:

Theorem 3 *Let* $\hat{\Gamma} = \{\mathcal{X} \in \mathbf{R}^2 : g_{color}(\mathcal{X}) = 0\}$ *be a simple Jordan curve of class* C^2 *and* $Dg(\mathcal{X}) = 0$ *in* $\hat{\Gamma}$. *Furthermore, assume* $u_0 \in W^{1,\infty}(\mathbf{R}^2) \cap \mathrm{BUC}(\mathbf{R}^2)$ *is of class* C^2 *and such that the set* $\{\mathcal{X} \in \mathbf{R}^2 : u_0(\mathcal{X}) \leq 0\}$ *contains* $\hat{\Gamma}$ *and its interior. Let* $u(t,\mathcal{X})$ *be the solution of (25) and* $\Gamma(t) = \{\mathcal{X} \in \mathbf{R}^2 : u(t,\mathcal{X}) = 0\}$. *Then, if* ν, *the constant component of the velocity, is sufficiently large,* $\Gamma(t) \to \hat{\Gamma}$ *as* $t \to \infty$ *in the Hausdorff distance.*

This theorem is proved in [14] for the minimal surfaces based model for 3D object segmentation. In this theorem, we assumed ν to be sufficiently large. A similar result can be proved for the basic geodesic model, that is for $\nu = 0$, assuming the maximal distance between $\hat{\Gamma}$ and the initial curve $\Gamma(0)$ is given and bounded (to avoid local minima).

5.2 Experimental results

We now present some examples of our vector snakes model. The numerical implementation is based on the algorithm for surface evolution via level-sets developed by Osher and Sethian [69, 88, 89] and recently used by many authors for different problems in computer vision and image processing. The algorithm allows the evolving curve to change topology without monitoring the deformation. Using new results in [1], the algorithm can be made to converge very fast. See the mentioned references for details on the numerics.

In our examples, the initialization is in general given by a curve surrounding all the possible objects in the scene. In the case of outward flows, a curve is initialized inside each object. Multiple initializations are performed in [57, 58, 95]. In [95], inner and outer active contours are simultaneously used. Although multiple initializations help in many cases, they may lead to false contours in noisy images. Therefore, multiple initializations should in general be controlled (by rough detections of points inside the objects for example) or they should be followed by a validation step.

Figure 2 presents an example of the geodesic active contours from [13]. The figure on the left is the original image, and the one on the right presents the evolving curves (green) and the detected boundaries (red). The initial curves are the two small circles in the tools. Both interior and exterior boundaries are detected without any special tracking procedure.

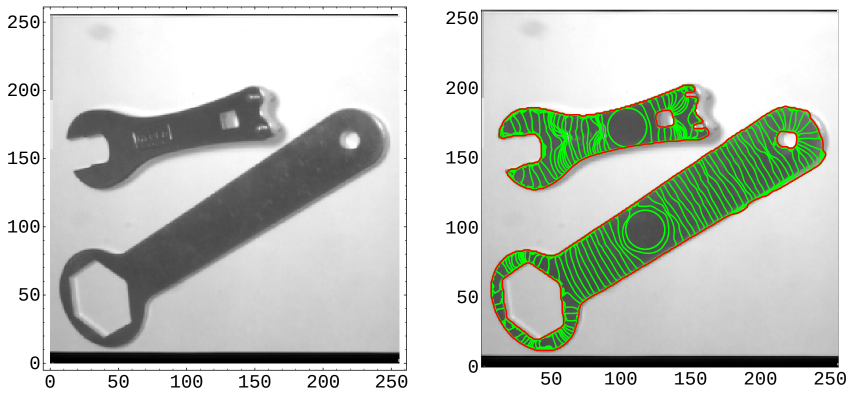

Figure 2: Example of the geodesic active contours. From the two small circles, both interior and exterior boundaries are detected without any special tracking procedure. (This is a color figure.)

In Figure 3 [4] we present the first example of the color snakes. The algorithm is applied to a color medical image (cryosections). Although the colors in medical data are in general pseudo-colors, they are associated to physical quantities, contain information and are correlated. Of course, in this case, the perceptual $L^*a^*b^*$ space has no meaning, and computations can be done on RGB space.

Another example is given in Figure 4 for a color image. The top row shows the three

[4] All the examples in this paper are presented without parameter optimization, showing the robustness of the framework here proposed. Results can be improved by selecting the appropriate parameters according to the image-type.

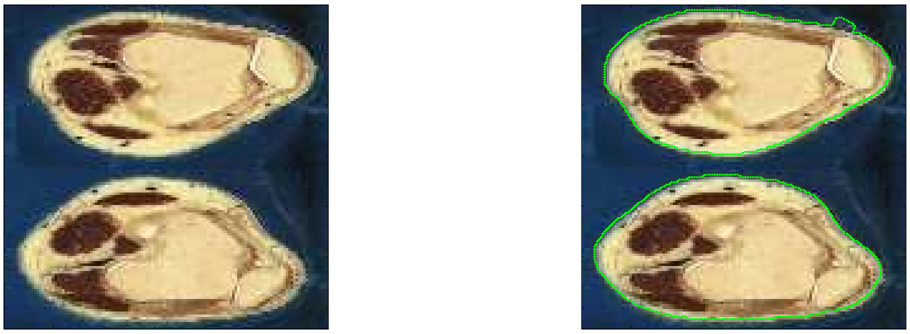

Figure 3: Example of the color geodesic active contours. The initial curve is a square surrounding both objects. The green curve is the result of the proposed algorithm. Both thighs are detected without any special topology handling procedures. (This is a color figure.)

planes corresponding to the RGB colors. The segmented hats obtained with the color snakes is given in the last raw.

In Figure 5 we present an outward flow for the color snakes. The initial contours are given by two circles in the dark background. These circles expand to detect the four objects, without tracking the topology of the evolving curve.

Figure 6 presents an example of the vector snakes for texture analysis. This shows an example of vector-valued data obtained from a single image. The original image is filtered with Gabor filters tuned to frequency and orientation as proposed in [52] for texture segmentation (see also [6, 107]). From this set of frequency/orientation decomposed images, g_{color} is computed according to the formulas in Section 4, and the vector-valued snakes flow is applied. [5] Four frequencies and four orientations are used, obtaining sixteen images. The results of this decomposition are shown in the 2nd to 5th raw (the original texture is shown in the first raw). The last raw shows the result of the vector snakes detecting one of the four textures boundaries. The original contour was a small circle inside it.

6 Color self-snakes

We extend now the formulation of the color geodesic snakes presented above to segmentation/simplification of vector-valued images. Related PDE/variational methods for grey-level image segmentation, as well as details on the approach described below for single-valued images, are given in [12].

[5] Further techniques for mixed color/texture segmentation based on the approach of vector-valued edges are being investigated by B. Rogoff and Y. Rubner as part of their PhD Thesis at Stanford University.

Figure 4: Example of the color snakes in a color image. The top row shows the three color planes RGB. The bottom row shows the result of the color snakes. (This is a color figure.)

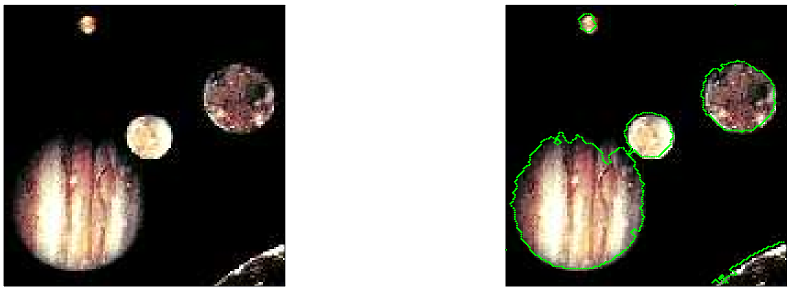

Figure 5: Outward flow of the color snakes. The initial curves are two circles on the dark background. These curves evolve outward to detect the four objects without any special topology tracking procedure. (This is a color figure.)

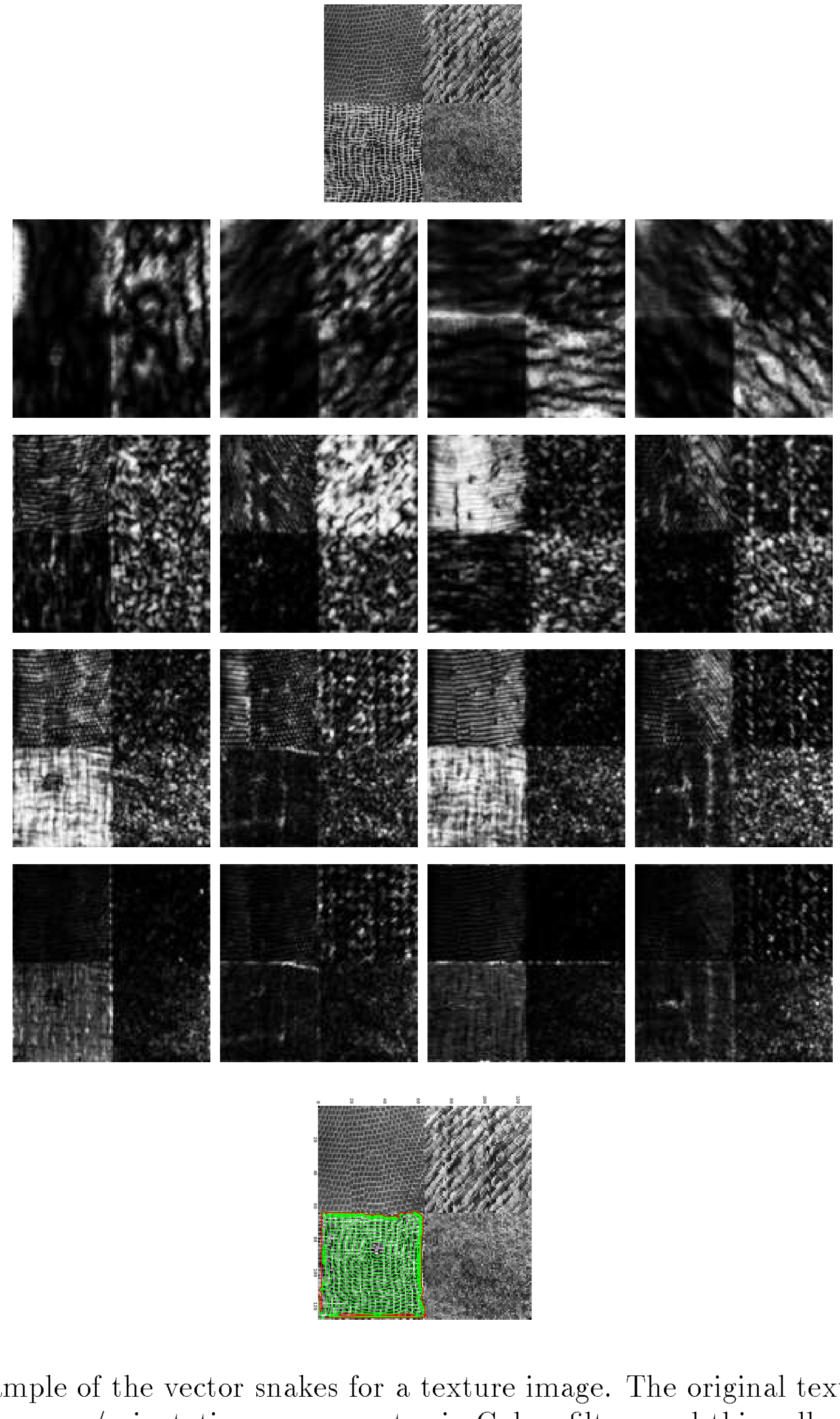

Figure 6: Example of the vector snakes for a texture image. The original texture is decomposed into frequency/orientation components via Gabor filters and this collection of images is used to compute the metric g_{color} for the snakes flow. The different components are shown, followed (last raw) by the result of the vector snakes, segmenting one of the texture boundaries (red contour). (This is a color figure.)

Observe the level-sets flow corresponding to the single-valued geodesic active contours, given by equation (11):

$$\begin{aligned}\frac{\partial u}{\partial t} &= |\nabla u| \mathrm{div}\left(g_{grey}(I)\frac{\nabla u}{|\nabla u|}\right)\\ &= g_{grey}(I)|\nabla u|\mathrm{div}\left(\frac{\nabla u}{|\nabla u|}\right) + \nabla g_{grey}(I)\cdot\nabla u.\end{aligned}$$

Two functions (maps from $I\!R^2$ to $I\!R$) are involved in this flow, the image I and the auxiliary level-sets one, u. Assume now $u \equiv I$, that is, the auxiliary level-sets function is the image itself. The equation above becomes

$$\begin{aligned}\frac{\partial I}{\partial t} &= |\nabla I| \mathrm{div}\left(g_{grey}(I)\frac{\nabla I}{|\nabla I|}\right) \qquad (26)\\ &= g_{grey}(I)|\nabla I|\mathrm{div}\left(\frac{\nabla I}{|\nabla I|}\right) + \nabla g_{grey}(I)\cdot\nabla I.\end{aligned}$$

A number of interpretations can be given to the equation above. First of all, based on the analysis of the geodesic active contours, the flow (26) indicates that each level-set of the image I moves according to the geodesic flow (10), being smoothly attracted by the term ∇g_{grey} to areas of high gradient. This gives the name of *self-snakes* to the flow; see [12].

Furthermore, (26) can be re-written as

$$\frac{\partial I}{\partial t} = \mathcal{F}_{diffusion} + \mathcal{F}_{shock}, \qquad (27)$$

where

$$\mathcal{F}_{diffusion} := g_{grey}(I)|\nabla I|\mathrm{div}\left(\frac{\nabla I}{|\nabla I|}\right),$$

$$\mathcal{F}_{shock} := \nabla g_{grey}(I)\cdot\nabla I.$$

The term $\mathcal{F}_{diffusion}$ is as in the anisotropic diffusion flow proposed in [3],

$$I_t = g_{grey}(I)|\nabla I|\mathrm{div}\left(\frac{\nabla I}{|\nabla I|}\right) = g_{grey} I_{\xi\xi},$$

where ξ is perpendicular to ∇I and $g_{grey}(I)$ is for example selected as in the snakes, according to (4). The idea is to smooth parallel to the edges (∇I) via $I_{\xi\xi}$ and "stop" the diffusion at high edges because of g_{grey}. We then have that the first part of (27) (or (26)), that is

$$I_t = \mathcal{F}_{diffusion},$$

is exactly the anisotropic diffusion given in [3]. This diffusion process is based on extending ideas originally presented by Perona & Malik [74]. Direct relation of (26) with the Perona-Malik flow will be given below as well (see also [2, 4, 106] and comments below).

Let us explain the second term in (27). This is straightforward from the geometric interpretation in Figure 1. The term $\nabla g_{grey} \cdot \nabla I$ "pushes" towards valleys of high gradients, acting as the shock-filter introduced in [70] for de-blurring. Therefore, the flow

$$I_t = \mathcal{F}_{shock},$$

is a shock-filter. We then obtain that the self-snakes given by (26) corresponds to a combination of anisotropic diffusion and shock filtering, further supporting its possible segmentation properties (for another combination of anisotropic diffusion and shock filtering see [4]). We have also obtained a variational-type interpretation to this filter, since the flow (26) may be associated to an energy analogue to L_R, where $\mathcal{C}$ is represented as level-sets of I and the integral is computed over the whole image. As we see next, variational interpretations to similar flows were previously reported [2, 38, 76, 106].

Let's now make a direct connection between the self-snakes and Perona-Malik flow. Perona and Malik [74] proposed the flow

$$\frac{\partial I}{\partial t} = \operatorname{div}\left(c_{grey}(I)\nabla I\right), \tag{28}$$

where c_{grey} is again an edge-stopping function as before. First of all note that the gradient descent of the energy (see for example [2, 38, 106])

$$\int\int h(|\nabla I|)dxdy$$

is given by

$$\frac{\partial I}{\partial t} = \operatorname{div}\left(h'(I)\frac{\nabla I}{|\nabla I|}\right). \tag{29}$$

Therefore, the Perona-Malik flow is minimizing this energy when $c_{grey} = \frac{h'(|\nabla I|)}{|\nabla I|}$. This property is extensively used in [106] to further analyze the flow. The total-variation approach [79] for example, is obtained for $h \equiv |\nabla I|$ (this case is well-posed, see below). The flow (28) may be ill-posed, for example when $c_{grey} = f(I)$ as originally proposed by Perona and Malik; see [3, 15, 65, 76, 106]. A way to solve this problem is to compute c_{grey} on a regularized version $\hat{I}$ of I [15]. Note that this is exactly what is done in the geodesic snakes and in the self-snakes presented above. (Other modifications to make the equation well-posed can be found in [65, 76, 104], as well as in [53, 79, 106].) Now comparing (28) with (26), we note that if $g_{grey} = h'$, the difference between the two flows is given by the gradient term $|\nabla I|$. Although this term can be "compensated" via the selection of g_{grey}, it is important to note it when comparing the self-snakes to Perona-Malik flow. The term $|\nabla I|$ affects both the diffusion part and the shock one.

The decomposition of the Perona-Malik flow in anisotropic diffusion and shock filtering parts was previously reported in [2, 106]. The authors in those papers show that the flow (29) is composed by a diffusion along the edges ($\mathcal{F}_{diffusion}$), which is the component in [3], and one perpendicular to the edges, giving a shock filter. Important and interesting analysis of the perpendicular component is given in [2, 106] as well (see also [4]). From the analysis performed in these works we learn that the self-snakes may be ill-posed depending on the selection of the function g_{grey}. Here we also showed the relation of those flows with the geodesic snakes and self-snakes. We refer the interested reader to the mentioned references for much deeper analysis of the Perona-Malik equation and its modifications.

Recapping, we have extended the geodesic active contours to a segmentation flow denoted as self-snakes, and briefly described its relations with previously reported image processing algorithms based on PDE's (see also [2, 4, 76, 79, 106]). The segmented image [6] is obtained as the steady state of the flow. See also [12] for details on the single valued self-snakes and its relation with other closely related approaches as the one in [90].

Let's now return to the segmentation of vector-valued images via *color self-snakes*. Being as before $\Phi : \mathbb{R}^2 \to \mathbb{R}^m$, we obtain a number of possible flows. The first one is based on combining the metric in the color snakes level-sets model (25) with the single-valued self-snakes (26), obtaining a system of coupled partial differential equations of the form $(i = 1, ..., m)$

$$\begin{aligned} \frac{\partial \Phi_i}{\partial t} &= |\nabla \Phi_i| \operatorname{div} \left(g_{color}(\Phi) \frac{\nabla \Phi_i}{|\nabla \Phi_i|} \right) \\ &= g_{color}(\Phi) |\nabla \Phi_i| \operatorname{div} \left(\frac{\nabla \Phi_i}{|\nabla \Phi_i|} \right) + \nabla g_{color}(\Phi) \cdot \nabla \Phi_i \\ &= g_{color}(\Phi) |\nabla \Phi_i| \kappa_{\Phi_i} + \nabla g_{color}(\Phi) \cdot \nabla \Phi_i. \end{aligned} \tag{30}$$

In this case, the color interaction is given by g_{color}, affecting the diffusion stopping term g_{color} as well as the shock-type one $\nabla g_{color}(\Phi) \cdot \nabla \Phi_i$. A different formulation can be obtained if $\nabla \Phi_i$ is replaced by the direction of maximal change $(\cos\theta_+, \sin\theta_-)$ and $|\nabla \Phi_i|$ by the color gradient $f(\lambda_\pm)$. The color self-snakes are related to the previously commented algorithms as well. It is of course related as well with the vector-valued extension of Perona-Malik approach presented in [103] and the work in [82].

The color self-snakes are tested in Figure 7 to show their behavior. In this image, $(\Phi_1, \Phi_2, \Phi_3) = (L^*, a, b)$ and g_{color} is computed based on the first fundamental form as discussed in Section 4. Since the goal is to present the framework for vector-valued segmentation, work is just directly performed on the color image in it $L^*a^*b^*$ representation. An immediate extension to improve the results will be to expand the vector space to $m > 3$ via frequency/orientation decompositions frequently used for texture segmentation [6, 52, 55, 107], which are important for color metrics as well [100]. Using the general approach in Section 4, the metric for this decomposed space can be computed as well. Figure 8 gives a second example. The original image is given in the first raw and the result of the color self-snakes in the second one (three different steps). To show the effect of the color shock filter ∇g_{color}, the last raw presents the same three steps of the self-snakes flow, with the term $\nabla g_{color} \cdot \nabla \Phi_i$ removed from the equation. This is very similar to the color diffusion flow described in this paper and introduced in [82]. The results of this self-snakes process can be used also as a rough first estimation for browsing on image date bases.

[6] By "segmented image" we refer to an image which has piecewise homogeneous (simplified) regions.

Figure 7: Example of the color self-snakes. The original image is given on the left and the steady state of the flow on the right. See text for details. (This is a color figure.)

7 Discussion and concluding remarks

In this paper we presented a novel framework of active contours for object segmentation in vector-valued images. The work is based on extending the results reported in [13] on geodesic snakes by means of defining a new metric in the vector space. We showed that the solution to the deformable contours approach for boundary detection is given by a geodesic curve in a Riemannian space defined by a metric derived from the given vector image. This means that detecting the object is equivalent to finding a curve of minimal weighted length. The weight is given by a definition of edges on vector-valued images, based on classical Riemannian geometry as in [82]. We also presented results regarding the existence, uniqueness, stability, and correctness of the solution obtained by our model.

Experiments for different real images were presented. Classical examples of imaging modalities were the proposed algorithm can be applied are color images and medical data. The scheme can be applied also to multi-valued data obtained from a single-valued image. For example, the multi-valued data can be composed from the original image at several scales, allowing a more robust segmentation. Frequency/orientation decompositions frequently used for texture segmentation [6, 52, 107] can define the vector image as well. Another example will be the combination of different image modalities as stereo, optical flow, and so on, as proposed in [95]. These modalities define again a vector-image, on which the combined metric can be computed using the technique reported in this work (a different metric is proposed in [95]). The sub-pixel accuracy intrinsic to the geodesic algorithm allows to perform accurate measurements after the object is detected [80].

The vector-valued object detection was then extended to obtain combined anisotropic diffusion and shock filtering in vector images. The flow is obtained by deforming each one of the image level sets according to the color geodesic flow. The relation between this algorithm and previously reported PDE based image processing ones was described. Relations between PDE-based algorithms were also reported in [2, 4, 106]. Here we added the geodesic snakes and self-snakes to the connection. This relation gives a number of different interpretations to the described flows as well as to those closely related to it. See also [12] and mentioned related references.

The work here described supports the importance of formulating problems as geodesic

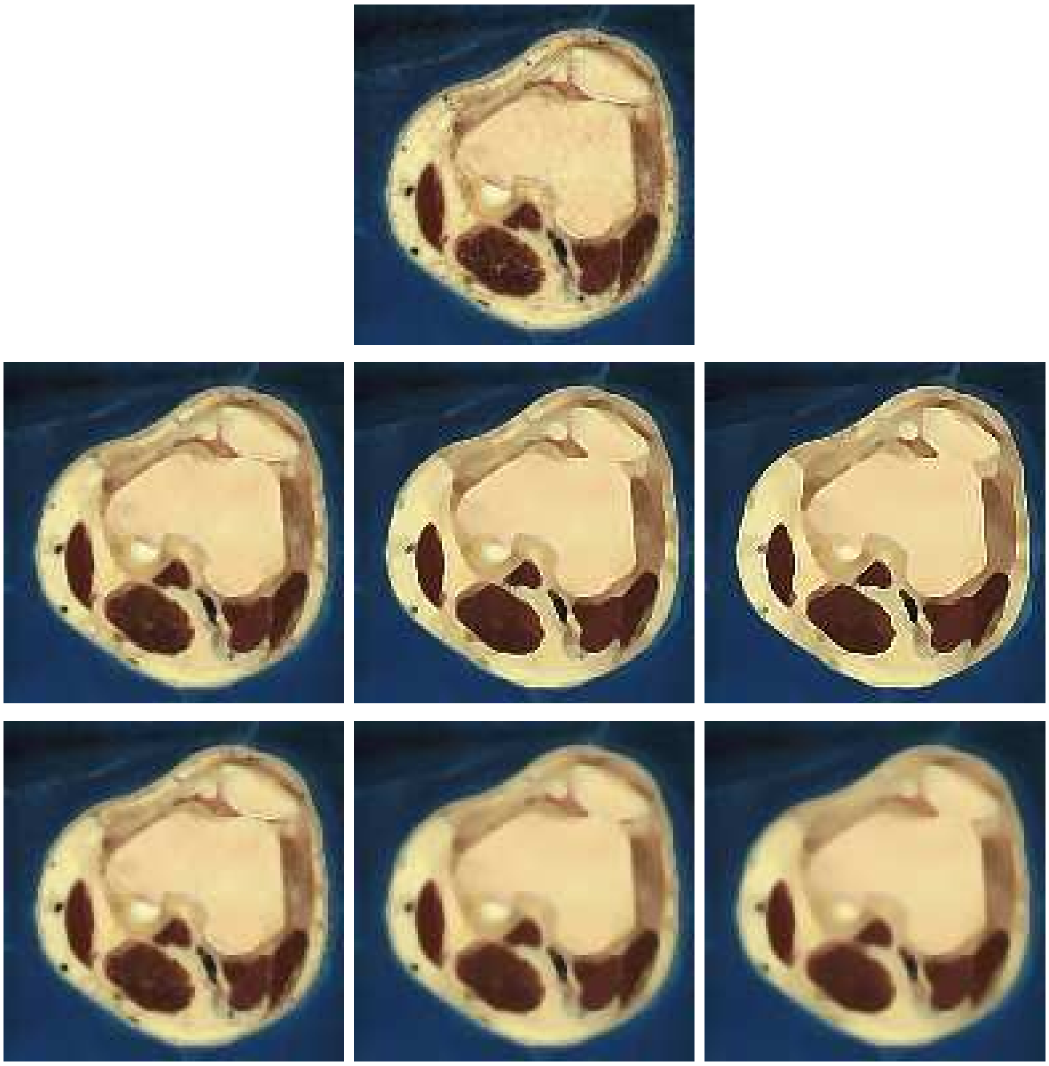

Figure 8: Example of the color self-snakes. First raw presents the original image, the second one three steps of the color self-snakes, and the last one again the color self-snakes without the shock part. (This is a color figure.)

computations [13, 42, 46, 47, 42, 66, 78]. The generality of the geodesic type formulation allows to perform a number of extensions, as the one presented in this paper. Other extensions include the affine invariant active contours introduced in [68]. This is based on defining a new metric which is affine invariant and allows to detect edges.

The color active contours here presented assumes the different image components are aligned. If the image components (planes) are not aligned, as in motion frames for example, we can use the 3D minimal surfaces approach [14] to simultaneously align and segment. The basic formulation in [14] (see also [42, 91]) is given by

$$\int g da,$$

where g is now the 3D metric and da the (Euclidean) element of area. The corresponding gradient descent flow for the 3D deforming surface $\mathcal{S}$ is then given by

$$\mathcal{S}_t = g\mathbf{H}\vec{\mathcal{N}} - \nabla g \cdot \vec{\mathcal{N}},$$

where $\mathbf{H}$ is the mean curvature of $\mathcal{S}$. If $g \equiv 1$, the classical formulation for minimal surfaces is obtained [71]. Assuming we have a series of 2D images $I(x, y, t)$ (t stands for the series) on each one we have to detect an object "moving" in between frames t. Then, we can define a new g that incorporates this information and solve the problem by computing 3D *spatio-temporal* minimal surfaces (Terzopoulos *at al.* [97] also define external forces for multi-frame images). For example, in the case of motion, g can be a function of the spatial gradient $\| \nabla_{\mathcal{X}} I(x, y, t) \| := \| I_x^2 + I_y^2 \|$ and the optical-flow (a time integrating term). The smoothness is automatically obtained as before due to the area term da. This topic is currently under investigation.

Acknowledgments

Color images in this paper are from the public domain image archives at MIT-Media Lab., Pusan National University, Delft University of Technology, Kodak PhotoCD, and the National Library of Medicine (The Visible Human Project). The grey-level image is courtesy of Prof. Andrew Zisserman from Oxford University. I wish to thank Dr. Dario Ringach from New York University for interesting discussions on color psychophysics and all his comments and teaching during our vector-diffusion research, Prof. David Mumford from Harvard University for pointing out the relation between "self-snakes" and Perona-Malik equation, Dr. Lenny Rudin from Cognitech Inc. for discussions on the shock effects of the ∇g term, Dr. Vicent Caselles from University of Illes Balears-Spain for all his comments and teaching during our collaboration on geodesics snakes and self-snakes, Dr. Ronny Kimmel from Technion-Israel for his insights and software support for the single-valued geodesic snakes, Brian Rogoff and Yossi Rubner from Stanford University for the Gabor-based texture decomposition data, Prof. Tony Chan from UCLA for comments on numerical algorithms to solve the vector-valued total variation, and Prof. Allen Tannenbaum from University of Minnesota, for all the interesting conversations on curve evolution we have since the first day of my PhD until today as well as his permanent support and encourage.

References

[1] D. Adalsteinsson and J. A. Sethian, "A fast level set method for propagating interfaces," *LBL TR-University of Berkeley*, December 1993.

[2] L. Alvarez, F. Guichard, P. L. Lions, and J. M. Morel, "Axioms and fundamental equations of image processing," *Arch. Rational Mechanics* **123**, 1993.

[3] L. Alvarez, P. L. Lions, and J. M. Morel, "Image selective smoothing and edge detection by nonlinear diffusion," *SIAM J. Numer. Anal.* **29**, pp. 845-866, 1992.

[4] L. Alvarez and L. Mazorra, "Signal and image restoration by using shock filters and anisotropic diffusion," *SIAM J. Numer. Anal.*, 1994.

[5] S. Angenent, "Parabolic equations for curves on surfaces, Part II. Intersections, blow-up, and generalized solutions," *Annals of Mathematics* **133**, pp. 171-215, 1991.

[6] C. Ballester and M. Gonzalez, "Texture discrimination by variational methods," *Technical Report*, U. of Illeas Balears, March 1995.

[7] M. J. Black and A. Rangarajan, "On the unification of line processes, outlier rejection, and robust statistics with applications in early vision," to appear *International Journal of Computer Vision.*

[8] A. Blake and A. L. Yuille (Ed.), *Active Vision*, MIT Press, Cambridge, MA, 1992.

[9] A. Blake and A. Zisserman, *Visual Reconstruction*, MIT Press, Cambridge, 1987.

[10] J. F. Canny, "A computational approach to edge detection," *IEEE-PAMI* **8**, pp. 679-698, 1986.

[11] V. Caselles, F. Catte, T. Coll, F. Dibos, "A geometric model for active contours," *Numerische Mathematik* **66**, pp. 1-31, 1993.

[12] V. Caselles, T. Coll, and G. Sapiro, "PDE's for image segmentation," in preparation.

[13] V. Caselles, R. Kimmel, and G. Sapiro, "Geodesic active contours," to appear *International Journal of Computer Vision.* A short version appears at *ICCV'95*, Cambridge, June 1995.

[14] V. Caselles, R. Kimmel, G. Sapiro, and C. Sbert, "Minimal surfaces: A three dimensional segmentation approach," *Technion EE Pub.* **973**, June 1995, submitted.

[15] F. Catte, P-L. Lions, J-M. Morel, and T. Coll, "Image selective smoothing and edge detection by nonlinear diffusion," *SIAM J. Numerical Analysis* **29**, pp.182-193, 1992.

[16] A. Chambolle, "Partial differential equations and image processing," to appear in *Proc. IEEE International Conference on Image Processing*, Texas, Austin, November 1994.

[17] Y. G. Chen, Y. Giga, and S. Goto, "Uniqueness and existence of viscosity solutions of generalized mean curvature flow equations," *J. Differential Geometry* **33**, pp. 749-786, 1991.

[18] D. Chopp, "Computing minimal surfaces via level set curvature flows," *LBL TR-University of Berkeley*, 1991.

[19] P. Cinquin, "Un modele pour la representation d'images medicales 3d," *Proc.. Euromedicine, Sauramps Medical*, **86**, pp 57-61, 1986.

[20] L. D. Cohen, "On active contour models and balloons," *CVGIP: Image Understanding* **53**, pp. 211-218, 1991.

[21] I. Cohen, L. D. Cohen, and N. Ayache, "Using deformable surfaces to segment 3D images and infer differential structure," *CVGIP: Image Understanding* **56**, pp. 242-263, 1992.

[22] L. D. Cohen and R. Kimmel, "Minimal geodesics of active contour models for edge integration and segmentation," pre-print, May 1995.

[23] M. G. Crandall, H. Ishii, and P. L. Lions, "User's guide to viscosity solutions of second order partial linear differential equations," *Bulletin of the American Math. Society* **27**, pp. 1-67, 1992.

[24] A. Cumani, "Edge detection in multispectral images," *CVGIP: Graphical Models and Image Processing* **53**, pp. 40-51, 1991.

[25] S. Di Zenzo, "A note on the gradient of a multi-image," *CVGIP* **33**, pp. 116-125, 1986.

[26] M. P. Do Carmo, *Differential Geometry of Curves and Surfaces*, Prentice-Hall, 1976.

[27] B. A. Dubrovin, A. T. Fomenko, and S. P. Novikov, *Modern Geometry - Methods and Applications I*, Springer-Verlag, New York, 1984.

[28] L. C. Evans and J. Spruck, "Motion of level sets by mean curvature, I," *J. Differential Geometry* **33**, pp. 635-681, 1991.

[29] O. Faugeras, "On the evolution of simple curves of the real projective plane," *Comptes rendus de l'Acad. des Sciences de Paris* **317**, pp. 565-570, September 1993.

[30] O. Faugeras, "Cartan's moving frame method and its application on the geometry and evolution of curves in the Euclidean, affine, and projective planes," *INRIA TR* **2053**, September 1993.

[31] O. Faugeras and R. Keriven, "Scale-spaces and affine curvature," *Proc. Europe-China Workshop on Geometrical Modeling and Invariants for Computer Vision*, R. Mohr and C. Wu (Eds.), pp. 17-24, 1995

[32] W. T. Freeman and E. H. Adelson, "The design and use of steerable filters," *IEEE-PAMI* **9**, pp. 891-906, 1991.

[33] P. Fua and Y. G. Leclerc, "Model driven edge detection," *Machine Vision and Applications,* **3**, pp. 45-56, 1990.

[34] M. Gage and R. S. Hamilton, "The heat equation shrinking convex plane curves," *J. Differential Geometry* **23**, pp. 69-96, 1986.

[35] D. Geman and G. Reynolds, "Constrained restoration and the recovery of discontinuities," *IEEE-PAMI* **14**, pp. 367-383, 1992.

[36] M. Grayson, "The heat equation shrinks embedded plane curves to round points," *J. Differential Geometry* **26**, pp. 285-314, 1987.

[37] H. W. Guggenheimer, *Differential Geometry,* McGraw-Hill Book Company, New York, 1963.

[38] F. Guichard, "Multiscale analysis of movies: Theory and algorithms," *PhD Dissertation*, CEREMADE-Paris, 1993.

[39] R. M. Haralick and L. G. Shapiro, "Image segmentation techniques," *Comp. Vision Graph. and Image Proc.* **29**, pp. 100-132, 1985.

[40] H. Helmholtz, von, *Handbuch der Psychologischen Optik* (2nd edition), Voss, Hamburg, 1896.

[41] M. Kass, A. Witkin, and D. Terzopoulos, "Snakes: Active contour models," *International Journal of Computer Vision* **1**, pp. 321-331, 1988.

[42] S. Kichenassamy, A. Kumar, P. Olver, A. Tannenbaum, and A. Yezzi, "Gradient flows and geometric active contour models," *Proc. ICCV*, Cambridge, June 1995.

[43] S. Kichenassamy, A. Kumar, P. Olver, A. Tannenbaum, and A. Yezzi, "Conformal curvature flows: From phase transitions to active vision," to appear *Archive for Rational Mechanics and Analysis.*

[44] B. B. Kimia, A. Tannenbaum, and S. W. Zucker, "Toward a computational theory of shape: An overview," *Lecture Notes in Computer Science* **427**, pp. 402-407, Springer-Verlag, New York, 1990.

[45] B. B. Kimia, A. Tannenbaum, and S. W. Zucker, "Shapes, shocks, and deformations, I," *International Journal of Computer Vision*, to appear.

[46] R. Kimmel and A. M. Bruckstein, "Tracking level sets by level sets: A method for solving the shape from shading problem," *CVIU*, 62(1):47-58, July, 1995.

[47] R. Kimmel, K. Siddiqi, B. B. Kimia, A. M. Bruckstein, "Shape from shading: Level set propagation and viscosity solutions," *International Journal of Computer Vision*, to appear.

[48] R. Kimmel, N. Kiryati, A. M. Bruckstein, "Distance maps and weighted distance transforms," *Journal of Mathematical Imaging and Vision,* Special Issue on Topology and Geometry in Computer Vision, to appear.

[49] T. Koller, G. Gerig, G. Szekely, and D. Dettwiler, "Multiscale detection of curvilinear structures in 2d and 3d image data," *Proc. ICCV*, Cambridge, June 1996.

[50] E. Kreyszig, *Differential Geometry*, University of Toronto Press, Toronto, 1959.

[51] H-C. Lee and D. R. Cok, "Detecting boundaries in a vector field," *IEEE Trans. Signal Proc.* **39**, pp. 1181-1194, 1991.

[52] T. S. Lee, D. Mumford, and A. L. Yuille, "Texture segmentation by minimizing vector-valued energy functionals: The coupled-membrane model," *Lecture Notes in Computer Science* **588**, *ECCV'92*, pp. 165-173, Springer-Verlag, 1992.

[53] P. L. Lions, S. Osher, and L. Rudin, "Denoising and debluring algorithms with constrained nonlinear PDE's," to appear in *SIAM J. Numer. Analysis.*

[54] D. L. MacAdam, "Visual sensitivities to color differences in daylight," *J. Opt. Soc. Am.* **32**, p. 247, 1942.

[55] J. Malik and P. Perona, "Preattentive texture discrimination with early vision mechanism," *J. Opt. Soc. Am. A* **7**, pp. 923-932, 1990.

[56] R. Malladi and J. A. Sethian, "A unified approach to noise removal, image enhancement, and shape recovery," pre-print, July 1995.

[57] R. Malladi, J. A. Sethian and B. C. Vemuri, "Evolutionary fronts for topology independent shape modeling and recovery," *Proc. of the 3rd ECCV*, Stockholm, Sweden, pp. 3-13, 1994.

[58] R. Malladi, J. A. Sethian and B. C. Vemuri, "Shape modeling with front propagation: A level set approach," *IEEE Trans. on PAMI,* January 1995.

[59] T. McInerney and D. Terzopoulos, "Topologically adaptable snakes," *Proc. ICCV*, Cambridge, June 1995.

[60] D. Metaxas and D. Terzopoulos, "Shape and nonrigid motion estimation trough physics-based synthesis," *IEEE-PAMI* **15**, pp. 580-591, 1993.

[61] J-M. Morel and S. Solimini, *Variational Methods in Image Segmentation,* Birkhauser, Boston, 1994.

[62] D. Mumford and J. Shah, "Optimal approximations by piecewise smooth functions and variational problems," *Comm. Pure and App. Math.* **42**, 1989.

[63] R. Nevatia, "A color edge detector and its use in scene segmentation," *IEEE Trans. Syst. Man, Cybern.,* **7**, pp. 820-826, 1977.

[64] W. J. Niessen, B. M. ter Haar Romeny, L. M. J. Florack, and A. H. Salden, "Nonlinear diffusion of scalar images using well-posed differential operators," Technical Report, Utrecht University, The Netherlands, October 1993.

[65] M. Nitzberg and T. Shiota, "Nonlinear image filtering with edge and corner enhancement," *IEEE Trans. PAMI* **14**, pp. 826-833, 1992.

[66] J. Oliensis and P. Dupuis, "Direct Method For Reconstructing Shape From Shading," *Proceedings SPIE Conf. 1570 on Geometric Methods in Computer Vision*, pp. 116-128, 1991.

[67] P. J. Olver, G. Sapiro, and A. Tannenbaum, "Differential invariant signatures and flows in computer vision: A symmetry group approach," in *Geometry Driven Diffusion in Computer Vision*, B. Romeny (Ed.), Kluwer, 1994.

[68] P. J. Olver, G. Sapiro, and A. Tannenbaum, "Affine invariant detection: Edges, active contours, and segments," in preparation.

[69] S. J. Osher and J. A. Sethian, "Fronts propagation with curvature dependent speed: Algorithms based on Hamilton-Jacobi formulations," *Journal of Computational Physics* **79**, pp. 12-49, 1988.

[70] S. Osher and L. I. Rudin, "Feature-oriented image enhancement using shock filters," *SIAM J. Numer. Anal.* **27**, pp. 919-940, 1990.

[71] R. Osserman, *Survey of Minimal Surfaces*, Dover, 1986.

[72] E. J. Pauwels, P. Fiddelaers, and L. J. Van Gool, "Shape-extraction for curves using geometry-driven diffusion and functional optimization," *Proc. ICCV*, Cambridge, June 1995.

[73] F. Perez and C. Koch, "Towards color image segmentation in analog VLSI: Algorithm and hardware," *International Journal of Computer Vision* **12**, pp. 17-42, 1994.

[74] P. Perona and J. Malik, "Scale-space and edge detection using anisotropic diffusion," *IEEE Trans. Pattern Anal. Machine Intell.* **12**, pp. 629-639, 1990.

[75] P. Perona and J. Malik, "Detecting and localizing edges composed of steps, peaks, and roofs," *MIT - CICS Technical Report*, October 1991.

[76] P. Perona, T. Shiota, and J. Malik, "Anisotropic diffusion," in [77].

[77] B. Romeny (Ed.), *Geometry Driven diffusion in Computer Vision*, Kluwer, 1994.

[78] E. Rouy and A. Tourin, "A viscosity solutions approach to shape-from-shading," *SIAM. J. Numer. Analysis* **29**, pp. 867-884, 1992.

[79] L. I. Rudin, S. Osher, and E. Fatemi, "Nonlinear total variation based noise removal algorithms," *Physica D* **60**, pp. 259-268, 1992.

[80] G. Sapiro, R. Kimmel, and V. Caselles, "Object detection and measurements in medical images via geodesic active contours," SPIE-Vision Geometry, San Diego, July 1995.

[81] G. Sapiro, R. Kimmel, D. Shaked, B. B. Kimia, and A. M. Bruckstein, "Implementing continuous-scale morphology via curve evolution," *Pattern Recog.* **26:9**, pp. 1363-1372, 1993.

[82] G. Sapiro and D. Ringach, "Anisotropic diffusion in color space," October 1994, submitted.

[83] G. Sapiro and A. Tannenbaum, "On affine plane curve evolution," *Journal of Functional Analysis* **119:1**, pp. 79-120, 1994.

[84] G. Sapiro and A. Tannenbaum, "Affine invariant scale-space," *International Journal of Computer Vision* **11:1**, pp. 25-44, 1993.

[85] G. Sapiro and A. Tannenbaum, "On invariant curve evolution and image analysis," *Indiana University Mathematics Journal* **42:3**, 1993.

[86] G. Sapiro and A. Tannenbaum, "Area and length preserving geometric invariant scale-spaces," *IEEE Trans. PAMI* **17:1**, pp. 67-72, 1995.

[87] E. Schrödinger, "Grundlinien einer Theorie der Farbenmetrik in Tagessehen," *Ann. Physik* **63**, p. 481, 1920.

[88] J. A. Sethian, "Curvature and the evolution of fronts," *Commun. Math. Phys.* **101**, pp. 487-499, 1985.

[89] J. A. Sethian, "A review of recent numerical algorithms for hypersurfaces moving with curvature dependent flows," *J. Differential Geometry* **31**, pp. 131-161, 1989.

[90] J. Shah, "Segmentation by nonlinear diffusion," *Proc. IEEE-CVPR*, 1991.

[91] J. Shah, "Recovery of shapes by evolution of zero-crossings," Technical Report, Math. Dept. Northeastern Univ. Boston MA, 1995.

[92] H.M. Soner, "Motion of a set by the curvature of its boundary," *J. of Diff. Equations* **101**, pp. 313-372, 1993.

[93] W. S. Stiles, "A modified Helmholtz line element in brightness-colour space," *Proc. Phys. Soc. (London)* **58**, p. 41, 1946.

[94] R. Szeliski, D. Tonnesen, and D. Terzopoulos, "Modeling surfaces of arbitrary topology with dynamic particles," *Proc. CVPR*, pp. 82-87, 1993.

[95] H. Tek and B. B. Kimia, "Image segmentation by reaction-diffusion bubbles," *Proc. ICCV*, Cambridge, June 1995.

[96] D. Terzopoulos and D. Metaxas, "Dynamic 3D models with local and global deformations: Deformable superquadrics," *IEEE-PAMI* **13**, pp. 703-714, 1991.

[97] D. Terzopoulos, A. Witkin, and M. Kass, "Constraints on deformable models: Recovering 3D shape and nonrigid motions," *Artificial Intelligence* **36**, pp. 91-123, 1988.

[98] V. Torre and T. Poggio, "On edge detection," *IEEE Trans. PAMI* **8**, pp. 147-163, 1986.

[99] J. J. Vos, and P. L. Walraven, "An analytical description of the line element in the zone-fluctuation model of colour vision. II. The derivation of the line element," *Vision Research* **12**, pp. 1345–1365, 1972.

[100] B. Wandell, *Foundations of Vision*, Sinauer, 1995.

[101] R. T. Whitaker, "Volumetric deformable models: Active blobs," *ECRC TR* **94-25**, 1994.

[102] R. T. Whitaker, "Algorithms for implicit deformable models," *Proc. ICCV'95*, Cambridge, June 1995.

[103] R. T. Whitaker and G. Gerig, "Vector-valued diffusion," in B. Romeny, Editor, *Geometry Driven Diffusion in Computer Vision*, Kluwer, 1994.

[104] R. T. Whitaker and S. M. Pizer, "A multi-scale approach to nonuniform diffusion," *CVGIP: Image Understanding* **57**, pp. 99-110, 1993.

[105] G. Wyszecki and W. S. Stiles, *Color Science: Concepts and Methods, Qualitative Data and Formulae*, (2nd edition), John Wiley & Sons, 1982.

[106] Yu-Li You, M. Kaveh, Wenyuan Xu, and A. Tannenbaum, "Analysis and design of anisotropic diffusion for image processing," *Proc. IEEE ICIP*, Austin, November 1994.

[107] S. C. Zhu, T. S. Lee, and A. L. Yuille, "Region competition: Unifying snakes, region growing, energy/Bayes/MDL for multi-band image segmentation," *Proc. ICCV*, Cambridge, June 1995.

[108] S. W. Zucker, "Region growing: Childhood and adolescence (survey)," *Comp. Vision Graph. and Image Proc.* **5**, pp. 382-399, 1976.

[109] S. W. Zucker and R. A. Hummel, "A three-dimensional edge operator," *IEEE-PAMI* **3**, pp. 324-331, 1981.